PHYSICAL REVIEW D **81,** 104028 (2010)

Gravitational-wave stochastic background from kinks and cusps on cosmic strings

S. Ölmez,[1] V. Mandic,[1] and X. Siemens[2]

[1]*Department of Physics and Astronomy, University of Minnesota, Minneapolis, Minnesota 55455, USA*

[2]*Center for Gravitation and Cosmology, Department of Physics, P.O. Box 413, University of Wisconsin-Milwaukee, Wisconsin 53201, USA*

(Received 15 April 2010; published 13 May 2010)

We compute the contribution of kinks on cosmic string loops to stochastic background of gravitational waves (SBGW). We find that kinks contribute at the same order as cusps to the SBGW. We discuss the accessibility of the total background due to kinks as well as cusps to current and planned gravitational-wave detectors, as well as to the big bang nucleosynthesis (BBN), the cosmic microwave background (CMB), and pulsar timing constraints. As in the case of cusps, we find that current data from interferometric gravitational-wave detectors, such as LIGO, are sensitive to areas of parameter space of cosmic string models complementary to those accessible to pulsar, BBN, and CMB bounds.

DOI: 10.1103/PhysRevD.81.104028 PACS numbers: 04.30.Db

I. INTRODUCTION

Topological defects are remnants of spontaneously broken local or global symmetries. The simplest and the most well-known example of the former one is the Abrikosov-Nielsen-Olesen flux tube [1], which originates from spontaneously broken $U(1)$ gauge symmetry. Most of the attention in the literature has been focused on defects originating from broken gauge symmetries, since grand unified theories have gauge symmetries which are eventually spontaneously broken down to the symmetry of the standard model. Cosmic strings are one-dimensional topological defects predicted by a large class of unified theories [2–4]. Cosmic strings were first considered as the seeds of structure formation [5,6], however, later, it was discovered that cosmic strings were incompatible with the cosmic microwave background (CMB) angular power spectrum. Cosmic strings can still contribute to structure formation, but they cannot be the dominant source. Cosmic strings are also candidates for the generation of other observable astrophysical phenomena such as high energy cosmic rays, gamma ray burst and gravitational waves [3,7–9]. Furthermore, recently it has been shown that in string-theory-inspired cosmological scenarios cosmic strings may also be generated [10]. They are referred to as cosmic superstrings. This realization has revitalized interest in cosmic strings and their potential observational signatures. There are some important differences between cosmic strings and cosmic superstrings. The reconnection probability is unity for cosmic strings [3,11]. Cosmic superstrings, on the other hand, have reconnection probability less than unity. This is a result of the probabilistic nature of their interaction and also the fact that it is less probable for strings to meet since they can live in higher dimensions [12]. The value of p ranges from 10^{-3} to 1 in different theories [13]. Cosmic superstrings could also be unstable, decaying long before the present time. In this case, however, they may also leave behind a detectable gravitational-wave signature [14].

In the early Universe, a network of cosmic strings evolves toward to an attractor solution called the ''scaling regime.'' In the scaling regime the statistical properties of the network, such as the average distance between strings and the size of loops at formation, scale with the cosmic time. In addition, the energy density of the network remains a small constant fraction of the energy density of the Universe. For cosmic superstrings in the scaling regime, the density of the network ρ is inversely proportional to the reconnection probability p, that is $\rho \propto p^{-\beta}$. The value of β is still under debate [15–17], and as a placeholder in our analysis we assume that $\beta = 1$.

The gravitational interaction of strings is characterized by their tension μ, or more conveniently by the dimensionless parameter $G\mu$, where G is Newton's constant. The current CMB bound on the tension is $G\mu < 6.1 \times 10^{-7}$ [18,19]. It was first believed that gravitational radiation from cosmic strings with $G\mu \ll 10^{7}$ would be too weak to observe. However it was later shown that gravitational radiation produced at cusps, which have large Lorentz boosts, could lead to a detectable signal [20–22]. Gravitational radiation bursts from (super)strings could be observable by current and planned gravitational-wave detectors for values of $G\mu$ as low as 10^{-13}, which may provide a test for a certain class of string theories [23]. Indeed, searches for burst signals using ground-based detectors are already underway [24].

A gravitational background produced by the incoherent superposition of cusp bursts from a network of cosmic strings and superstrings was considered in [25]. In this paper we extend this computation to include kinks, long-lived sharp edges on strings that result from intercommutations, and find that kinks contribute at almost the same level as cusps. We investigate the detectability of the total background produced by cusps and kinks by a wide range of current and planned experiments. A similar calculation for the case of infinite strings has been undertaken in the recent paper [26]; see also [27].

The organization of the paper is as follows: In Sec. II we consider gravitational waves generated by cusps and kinks in the weak field limit [28]. In this section we follow the conventions of [20,21], and more details can be found in these references. In Sec. III we derive the expression for the stochastic background, which is a double integral over redshift and loop length. In Sec. IV we evaluate the integral analytically with certain approximations, which results in a flat distribution for larger values of the frequency. Finally in Sec. V we numerically evaluate the background and discuss the observability by various experiment.

II. GRAVITATIONAL RADIATION

In this section we consider gravitational waves created by cusps and kinks. For completeness we follow closely the analysis in [20,21], and reproduce a number of their results. We begin with a derivation for the metric perturbation in terms of the Fourier transform of the stress-energy tensor of the source. We then write the stress-energy tensor for a relativistic string and compute its Fourier transform. Using these results we then compute the gravitational waveforms produced by cusps and kinks on cosmic strings.

A. Calculation of metric perturbations

Gravitational waves from a source can be calculated using the weak field approximation [28],

$$g_{\mu\nu} = \eta_{\mu\nu} + h_{\mu\nu}, \tag{1}$$

where $\eta_{\mu\nu}$ is the Minkowski metric with positive signature and $h_{\mu\nu}$ is the metric perturbation. In the harmonic gauge, $g^{\mu\nu}\Gamma^{\lambda}_{\mu\nu} = 0$, the linearized Ricci tensor is

$$R_{\mu\kappa} \simeq \frac{1}{2}\partial_\lambda\partial^\lambda h_{\mu\kappa}. \tag{2}$$

Substituting into Einstein's equations yields

$$R_{\mu\nu} - \frac{1}{2}g_{\mu\nu}R \simeq \frac{1}{2}\left(\partial_\lambda\partial^\lambda h_{\mu\nu} - \frac{1}{2}\eta_{\mu\nu}\partial_\lambda\partial^\lambda h\right) = -8\pi G\mathcal{T}_{\mu\nu}, \tag{3}$$

where R is the Ricci scalar, $\mathcal{T}_{\mu\nu}$ is the energy-momentum tensor of matter, and $h = \eta_{\mu\nu}h^{\mu\nu}$. Defining $\bar{h}_{\mu\nu} = h_{\mu\nu} - \frac{1}{2}\eta_{\mu\nu}h$ further simplifies Eq. (3),

$$\partial_\lambda\partial^\lambda\bar{h}_{\mu\nu} = -16\pi G\mathcal{T}_{\mu\nu}, \tag{4}$$

which is a wave equation with a source term. We can rewrite this equation in the frequency domain as

$$(w^2 + \nabla^2)\bar{h}_{\mu\nu}(\vec{x}, w) = -16\pi G\mathcal{T}_{\mu\nu}(x, w), \tag{5}$$

where

$$\bar{h}_{\mu\nu}(\vec{x}, w) = \int dt e^{iwt}\bar{h}_{\mu\nu}(\vec{x}, t). \tag{6}$$

Equation (5) can be solved by using Green's function for the operator $w^2 + \nabla^2$, which is

$$\mathcal{G}(\vec{x} - \vec{x}', w) = \frac{e^{iw|\vec{x}-\vec{x}'|}}{|\vec{x} - \vec{x}'|}. \tag{7}$$

Therefore metric perturbations are given by

$$\bar{h}_{\mu\nu}(\vec{x}, w) = -16\pi G\int d^3x'\mathcal{G}(\vec{x} - \vec{x}', w)\mathcal{T}_{\mu\nu}(\vec{x}', w) = -16\pi G\frac{e^{iw|\vec{x}|}}{|\vec{x}|}\mathcal{T}_{\mu\nu}(\vec{k}, w), \tag{8}$$

where $\vec{k} = w\hat{x}$ and

$$\mathcal{T}_{\mu\nu}(\vec{k}, w) = \frac{1}{T}\int_0^T dt\int d^3x' e^{i(wt - \vec{k}\cdot\vec{x}')}\mathcal{T}_{\mu\nu}(\vec{x}', t), \tag{9}$$

where T is the fundamental period of the source. Equation (8) relates energy-momentum tensor to gravitational waves. The next step is to calculate the energy-momentum tensor of cusps and kinks on cosmic strings.

B. Energy-momentum tensor of cosmic strings

In the thin wire approximation, the dynamics of strings is described by the Nambu-Goto action [3,7]

$$S = -\mu\int d\tau d\sigma\sqrt{-\gamma}, \tag{10}$$

where σ and τ are world-sheet coordinates and μ is the string tension. γ is the determinant of the induced metric

$$\gamma_{ab} = \eta_{\mu\nu}\partial_a X^\mu\partial_b X^\nu, \tag{11}$$

where a and b denote world-sheet coordinates. The equation of motion following from Eq. (10) is

$$(\partial_\tau^2 - \partial_\sigma^2)X^\mu = 0. \tag{12}$$

The solution must also satisfy Virasoro conditions

$$\dot{X}\cdot\dot{X} + X'\cdot X' = 0 \quad \text{and} \quad \dot{X}\cdot X' = 0, \tag{13}$$

where *dot* and *prime* denote derivatives with respect to τ and σ, respectively. If we define $\sigma_\pm = \tau \pm \sigma$, the equation of motion becomes

$$\partial_+\partial_- X^\mu = 0, \tag{14}$$

which is solved by left- and right-moving waves,

$$X^\mu = \frac{1}{2}(X_+^\mu(\sigma_+) + X_-^\mu(\sigma_-)). \tag{15}$$

Furthermore Virasoro conditions in Eq. (13) simplify to

$$\dot{\mathbf{X}}_\pm^2 = 1, \tag{16}$$

where *dot* now represents the derivative with respect to the (unique) argument of the functions $X_\pm^\mu$. We require that $X^\mu(\sigma, \tau)$ is periodic in σ with period l, which is the length of the loop. This implies that the functions $X_\pm^\mu$ are periodic functions with the same period. The period in t is $l/2$ since

$X^\mu(\sigma + l/2, \tau + l/2) = X^\mu(\sigma, \tau)$. The energy-momentum tensor corresponding to the Nambu-Goto action can be calculated by varying Eq. (10) with respect to the metric, which yields

$$\begin{aligned}\mathcal{T}_{\mu\nu}(x) &= -2\frac{\delta S}{\delta \eta_{\mu\nu}} \\ &= \mu \int d\tau d\sigma (\dot{X}^\mu \dot{X}^\nu - X'^\nu X'^\mu)\delta^{(4)}(x - X) \\ &= \frac{\mu}{2}\int d\sigma_- d\sigma_+ (\dot{X}^\mu_+ \dot{X}^\nu_- + \dot{X}^\nu_- \dot{X}^\mu_-)\delta^{(4)}(x - X).\end{aligned} \tag{17}$$

Inserting this expansion into Eq. (9) gives us the energy-momentum tensor in momentum space

$$\mathcal{T}_{\mu\nu}(k) = \frac{\mu}{T_l}\int d\sigma_- d\sigma_+ \dot{X}^{(\mu}_+ \dot{X}^{\nu)}_- e^{-(i/2)(k\cdot X_+ + k\cdot X_-)}, \tag{18}$$

where we define

$$\dot{X}^{(\mu}_+ \dot{X}^{\nu)}_- = \frac{1}{2}(\dot{X}^\mu_+ \dot{X}^\nu_- + \dot{X}^\mu_- \dot{X}^\nu_+). \tag{19}$$

The nice property of Eq. (18) is that two integrals can be calculated independently,

$$I^\mu_\pm(k) \equiv \int_0^l d\sigma_\pm \dot{X}^\mu_\pm e^{-(i/2)k\cdot X_\pm}, \tag{20}$$

and the energy-momentum tensor can be expressed in terms of $I^\mu_\pm$ as follows:

$$\mathcal{T}_{\mu\nu}(k) = \frac{\mu}{l} I^{(\mu}_+ I^{\nu)}_-, \tag{21}$$

where we used $T_l = \frac{l}{2}$. In the following subsection we calculate $I^\mu_\pm$ for cusps and kinks.

1. Cusps

Let us start with the geometrical interpretation of Eq. (16). It tells us that $\dot{\mathbf{X}}_\pm$ trace a unit sphere centered at the origin, which is called Kibble-Turok sphere. Integrating $\dot{\mathbf{X}}_\pm$ and using the periodicity, we get

$$\int_0^l \dot{\mathbf{X}}_\pm(\sigma_\pm) d\sigma_\pm = 0, \tag{22}$$

which implies that $\dot{\mathbf{X}}_\pm$ cannot lie completely in a single hemisphere and therefore they intersect at some point(s). We choose our parametrization and the coordinate system such that the intersection occurs at the parameters $\sigma_\pm = 0$ at the origin, that is $X^\mu_\pm(0) = 0$. $X_\pm(\sigma_\pm)$ and $\dot{X}_\pm(\sigma_\pm)$ can be expanded around $\sigma_\pm = 0$

$$X^\mu_\pm(\sigma_\pm) = l^\mu_\pm \sigma_\pm + \frac{1}{2}\ddot{X}^\mu_\pm \sigma^2_\pm + \frac{1}{6}X^{(3)\mu}_\pm \sigma^3_\pm \tag{23}$$

$$\dot{X}^\mu_\pm(\sigma_\pm) = l^\mu_\pm + \ddot{X}^\mu_\pm \sigma_\pm + \frac{1}{2}X^{(3)\mu}_\pm \sigma^2_\pm, \tag{24}$$

where $l^\mu_\pm = \dot{X}^\mu_\pm(0)$. We can easily find the shape of $X^\mu_\pm$ at $\tau = 0$ ($\sigma_\pm = \pm\sigma$),

$$\begin{aligned}X^\mu(\sigma, \tau = 0) &= \frac{1}{2}(X^\mu_+(\sigma) + X^\mu_-(-\sigma)) \\ &= \frac{1}{4}(\ddot{X}^\mu_+ + \ddot{X}^\mu_-)\sigma^2 + \frac{1}{12}(X^{(3)\mu}_+ + X^{(3)\mu}_-)\sigma^3.\end{aligned} \tag{25}$$

In order to visualize the shape of the string around the origin, we can choose the coordinate system such that $(\ddot{\vec{X}}_+ + \ddot{\vec{X}}_-)$ lies on the x-axis, and define $x = \frac{1}{4}|\ddot{\vec{X}}_+ + \ddot{\vec{X}}_-|\sigma^2$. Let us also denote the direction of $\vec{X}^{(3)}_+ + \vec{X}^{(3)}_-$ by $\hat{y}$, which is not necessarily orthogonal to $\hat{x}$. If we define $y = \frac{1}{12}|X^{(3)\mu}_+ + X^{(3)\mu}_-|\sigma^3$, we see that $y \propto x^{3/2}$, which has a sharp turn at $x = 0$, which is referred to as cusp. We can calculate $I^\mu_\pm$ for cusps using the expansion in Eq. (23). First of all, we note that the first term of Eq. (24) is pure gauge; it can be removed by a coordinate transformation. Furthermore imposing the Virasoro condition in Eq. (16) gives

$$l_\pm \cdot \ddot{X}_\pm = 0, \quad \text{and} \quad 1_\pm \cdot \mathrm{X}^{(3)}_\pm = -\ddot{\mathrm{X}}^2_\pm. \tag{26}$$

When the line of sight k is in the direction of l we have $k = wl$, which gives $-ik\cdot X_\pm = \frac{i}{6}w\ddot{X}^2_\pm \sigma^3_\pm$. If we plug in the expansion in Eq. (23) into Eq. (20) we get

$$I^\mu_\pm(k) = \ddot{X}^\mu_\pm \int_0^l d\sigma \sigma e^{(i/12)w\ddot{X}^2_\pm \sigma^3} = \frac{2\pi i \ddot{X}^\mu_\pm}{3\Gamma(1/3)(\frac{1}{12}w|\ddot{X}^2_\pm|)^{2/3}}. \tag{27}$$

Replacing w with $2\pi f$ gives

$$I^\mu_\pm(k) = C^\mu_\pm f^{-(2/3)}, \tag{28}$$

$$\mathcal{T}_{\mu\nu}(k) = \frac{\mu}{l}|f|^{-(4/3)} C^{(\mu}_+ C^{\nu)}_-, \tag{29}$$

where $C^\mu_\pm = i\frac{(32\pi/3)^{1/3}}{\Gamma(1/3)}\frac{\ddot{X}^\mu_\pm}{|\ddot{X}_\pm|^{4/3}}$. Finally we need to estimate $|\ddot{X}_\pm| = |\ddot{\mathbf{X}}_\pm|$. Since $\mathbf{X}_\pm$ is periodic with period l, $\dot{\mathbf{X}}$ expanded as

$$\dot{\mathbf{X}}(\sigma_\pm) = \sum_n \mathbf{c_n} e^{i(2\pi/l)n\sigma_\pm}, \tag{30}$$

where the expansion coefficients $\mathbf{c_n}$ are constrained by $|\dot{\mathbf{X}}_\pm| = 1$. If the string is not too wiggly, $\mathbf{c_n}$ is nonvanishing for only small n, therefore we can estimate $|\ddot{X}_\pm| \sim \frac{2\pi}{l}$. Combining all the pieces together and neglecting decimal points in the numerical coefficient, we express the trace of the metric perturbations as

$$h^{(c)}(f) \equiv |\bar{h}^\mu_\mu| = \frac{G\mu l^{2/3}}{r}|f|^{-(4/3)}. \tag{31}$$

We can express r as a function of z

$$r = \frac{1}{H_0}\int_0^z \frac{dz'}{\mathcal{H}(z')} \equiv \frac{1}{H_0}\varphi_r(z), \tag{32}$$

where H_0 is the Hubble constant today and $\mathcal{H}(z)$ is the Hubble function given by

$$\mathcal{H}(z) = (\Omega_M(1+z)^3 + \Omega_R(1+z)^4 + \Omega_\Lambda)^{1/2}. \tag{33}$$

The numerical values for the constants in this equation are $\Omega_M = 0.25$, $\Omega_R = 4.6 \times 10^{-5}$, $\Omega_\Lambda = 1 - \Omega_R - \Omega_M$, and $H_0 = 73\,\mathrm{km/s/Mpc}$. Note that f in Eq. (31) is the frequency of the radiation in the frame of emission. In order to convert it to the frequency we observe today, the effect of the cosmological redshift must be included. The frequency in the frame of emission, f, is related to the frequency we observe now, f_{now}, by the relation $f = (1+z)f_{\mathrm{now}}$. After redshifting properly,[1] Eq. (31) becomes

$$h^{(c)}(f, z, l) = \frac{G\mu H_0 l^{2/3}}{(1+z)^{1/3}\varphi_r(z)}|f|^{-(4/3)}, \tag{34}$$

where we dropped the subscript "now."

2. Kinks

Calculation of kink radiation is similar to the cusp case. The form of I^μ_+ is the same as the cusp result. I^μ_- has a discontinuity at the cusp point and needs a different treatment. Let us describe the kink (at $\sigma_- = 0$ and $X_\pm = 0$) as a jump of the tangent vector from l^μ_1 to l^μ_2. At the first order one can replace approximate $\dot{X}^\mu_-$ by l^μ_1 for $\sigma_- < 0$ and l^μ_2 for $\sigma_- > 0$. At this approximation, one gets

$$I^\mu_-(k) = \int_{-l/2}^{l/2} d\sigma_- \dot{X}^\mu_- e^{-(i/2)k\cdot X_-} \simeq \frac{2i}{w}\left(\frac{l^\mu_1}{l_1\cdot\hat{k}} - \frac{l^\mu_2}{l_2\cdot\hat{k}}\right), \tag{35}$$

where we dropped two oscillatory terms. The exact value of Eq. (35) depends on the sharpness of the kink, $l_1 \cdot l_2$ [29], however we will assume that the average value of this quantity is of order one. Combining this result with I^μ_+ we get the frequency distribution of the radiation from a kink as

$$h^{(K)}(f, z, l) = \frac{G\mu l^{1/3} H_0}{(1+z)^{2/3}\varphi_r(z)} f^{-5/3}. \tag{36}$$

It is important to note that in the derivation of Eqs. (34) and (36) we assumed that the line of sight k^μ is in the direction of the motion of the cusp or kink, l^μ. It is easy to show that $I_\pm$ [Eq. (20)] decay exponentially with the angle between $\mathbf{k}$ and $\boldsymbol{l}$ [21]. Therefore Eqs. (34) and (36) are valid for angles smaller than

$$\theta_m = \frac{1}{(fl(1+z))^{1/3}}. \tag{37}$$

We implement this condition with a Θ-function in the amplitude.

III. STOCHASTIC BACKGROUND

The stochastic gravitational background [25] is given by

$$\Omega_{gw}(f) = \frac{4\pi^2}{3H_0^2} f^3 \int dz \int dl h^2(f, z, l)\frac{d^2R(z, l)}{dzdl}, \tag{38}$$

where $h(f, z, l)$ is given in Eqs. (34) and (36) and $\frac{d^2R(z,l)}{dzdl}$ is the observable burst rate per length per redshift, which will be defined below. We take the number of cusps (kinks) to be one per loop. (We will discuss how the number of cusps or kinks affects the stochastic background of gravitational waves [SBGW] in Sec. IV.) If we define the density (per volume) of the loops of length l at time t as $n(l, t)$, the rate of burst (per loop length per volume) can be expressed as $\frac{n(l,t)}{l/2}$, where $l/2$ factor is the fundamental period of the string. However, this is not the observable burst rate since we can observe only the fraction of bursts that is beamed toward us. Including this fraction we obtain

$$\frac{dR}{dldz} = H_0^{-3}\varphi_V(z)(1+z)^{-1}\frac{2n(l,t)}{l}\Delta(z, f, l), \tag{39}$$

where $(1+z)^{-1}$ comes from converting emission rate to observed rate, and $H_0^{-3}\varphi_V(z)$ follows from converting differential volume element to the corresponding function of redshift z,

$$dV = 4\pi a^3(t) r^2 dr = \frac{4\pi H_0^{-3}\varphi_r^2(z)}{(1+z)^3\mathcal{H}(z)}dz \equiv H_0^{-3}\varphi_V(z)dz, \tag{40}$$

where $a(t)$ is the cosmological scale factor. $\Delta(z, f, l)$ is the fraction of the bursts we can observe. Geometrically the radiation from a cusp will be in a conic region with half opening angle θ_m [Eq. (37)] and outside the cone it will decay exponentially. To simplify the calculation we assume that the radiation amplitude vanishes outside this conic region, which will be implemented by a Θ function. We can express the corresponding solid angle in terms of the opening angle by using the following relation:

$$\Omega_m = 2\pi(1 - \cos\theta_m) \simeq \pi\theta_m^2. \tag{41}$$

Thus the probability that the line of sight is within this solid angle is

$$\frac{\Omega_m}{4\pi} \simeq \theta_m^2/4, \tag{42}$$

[1] One should note that replacing f in Eq. (31) with $(1+z)f_{\mathrm{now}}$ is *not* correct, since this replacement will scale the argument and the amplitude of $h^{(c)}(f)$ by a factor of $\frac{1}{1+z}$, which is the reflection of the fact that the measure of Fourier integral is not dimensionless. Since redshifting should change the argument but not the amplitude, one needs to multiply the result by $1+z$ so that the amplitude remains the same. Equivalently, one can define the logarithmic Fourier transform, as discussed in Ref. [20], such that the measure of the transform becomes dimensionless.

which is referred to as the beaming fraction of the cusp. We combine the cutoff for large angles and beaming effect into

$$\Delta(z, f, l) \approx \frac{\theta_m^2(z, f, l)}{4}\Theta(1 - \theta_m(z, f, l)). \quad (43)$$

It is important to note that cusps are instantaneous events, and it is possible to observe their radiation only if the line of sight happens to be inside the cone of radiation. The beaming fraction, Eq. (42), which is proportional to θ_m^2, is the fraction of the time the line of sight is inside the cone of radiation. In contrast, kinks radiate continuously—as kinks travel around a string loop they radiate in a fanlike pattern. Therefore the radiation cone of a kink will sweep a strip of width $2\theta_m$ and an average length π on the surface of the unit sphere as it travels around the cosmic string loop. That is, the probability of observing radiation from a kink is

$$\frac{\Omega_m^c}{4\pi} \simeq \frac{2\theta_m \pi}{4\pi} = \frac{\theta_m}{2}. \quad (44)$$

For kinks the cutoff for large angles and beaming factor that enters the rate is therefore

$$\Delta^{(K)}(z, f, l) \approx \frac{\theta_m(z, f, l)}{2}\Theta(1 - \theta_m(z, f, l)). \quad (45)$$

Inserting this result into Eq. (38) gives the background radiation $\Omega_{gw}(f)$ as a double integral over l and z, which needs to be evaluated numerically. Finally we need to discuss the form of the loop density, $n(l, t)$ in Eq. (39). To do this, it is convenient to first convert the cosmic time t to a suitable function of redshift z using the following relation:

$$\frac{dz}{dt} = -(1 + z)H_0\mathcal{H}(z), \quad (46)$$

which can be integrated to give

$$t = H_0^{-1}\int_z^\infty \frac{dz'}{(1 + z')\mathcal{H}(z')} = H_0^{-1}\varphi_t(z). \quad (47)$$

Below we discuss the two main contending scenarios for the size of cosmic string loops.

A. Small loops

Early simulations suggested that the size of loops was dictated by gravitational backreaction. In this case the size of the loops is fixed by the cosmic time t, and all the loops present at a cosmic time t are of the same size αt. The value of α is set by the gravitational backreaction, that is $\alpha \propto \Gamma G\mu$ (in Sec. V we parametrize α by $\alpha = \epsilon\Gamma G\mu$ where ϵ is a parameter we scan over). The constant Γ is the ratio of the power radiated into gravitational waves by loops to $G\mu^2$. Numerical simulation results suggest that $\Gamma \sim 50$. Therefore the density is of the form

$$n(l, t) \propto (p\Gamma G\mu)^{-1}t^{-3}\delta(l - \alpha t), \quad (48)$$

where p is the reconnection probability. The overall coefficient is estimated by simulations (for a review, see [3]) which show that the density in the radiation domination era is about 10 times larger than the one in the matter domination era. This behavior of the density can be implemented by a function, $c(z)$, which converges to 10 for $z \gg z_{\rm eq}$ and to 1 for $z \ll z_{\rm eq}$. Therefore the density can be written as

$$n(l, t) = c(z)(p\Gamma G\mu)^{-1}t^{-3}\delta(l - \alpha t), \quad (49)$$

where [20]

$$c(z) = 1 + \frac{9z}{z + z_{\rm eq}}. \quad (50)$$

Such a distribution simplifies the calculation of SBGW since the l-integral in Eq. (38) can be evaluated trivially to yield

$$\begin{aligned}\Omega_{gw}(f) &= \frac{4\pi^2}{3H_0^2}\int dz \int dl h^2(f, z, l)\frac{d^2R(z, l)}{dzdl} \\ &= \frac{2cG\mu\pi^2 H_0^{1/3}}{3p\alpha^{1/3}\Gamma f^{1/3}} \\ &\quad \times \int dz \frac{c(z)\varphi_V\Theta(1 - [f(1 + z)\alpha\varphi_t]^{-1/3})}{(1 + z)^{7/3}\varphi_r^2\varphi_t^{10/3}}. \quad (51)\end{aligned}$$

For kinks, we have a similar integral,

$$\begin{aligned}\Omega_{gw}^K(f) &= \frac{4cG\mu\pi^2 H_0^{1/3}}{3p\alpha^{2/3}\Gamma f^{2/3}} \\ &\quad \times \int dz \frac{c(z)\varphi_V\Theta(1 - [f(1 + z)\alpha\varphi_t]^{-1/3})}{(1 + z)^{8/3}\varphi_r^2\varphi_t^{11/3}}. \quad (52)\end{aligned}$$

We analytically evaluate the integrals in Eqs. (51) and (52) in Sec. IV with certain approximations, and perform numerical integration in Sec. V.

B. Large loops

Recent simulations [30–32] suggest that the size of the loops is set by the large-scale dynamics of the network, and that the gravitational backreaction scale is irrelevant. It is important to emphasize that the sizes of large loops, which are set by the value of α, are still under debate. References [30,31] suggest lower values of α, whereas in Ref. [32] it is found that the loop production functions have peaks around $\alpha \approx 0.1$. The dependence of SBGW on α can be found in Sec. IV. In order to contrast the large loop and the small loop cases, we adopt $\alpha = 0.1$ for numerical computations.

For long-lived loops, the distribution can be calculated if a scaling process is assumed (see [3]). In the radiation era it is

$$n(l,t) = \chi_r t^{-(3/2)}(l + \Gamma G\mu t)^{-(5/2)}, \qquad l < \alpha t, \qquad t < t_{t_{\rm eq}}, \tag{53}$$

where $\chi_r \approx 0.4\zeta\alpha^{1/2}$, and ζ is a parameter related to the correlation length of the network [22]. The numerical value of ζ is found in numerical simulations of radiation era evolution to be about 15 (see Table 10.1 in [3]). The upper bound on the length arises because no loops are formed with sizes larger than αt. For $t > t_{\rm eq}$ (the matter era) the distribution has two components, loops formed in the matter era and survivors from the radiation era. Loops formed in the matter era have lengths distributed according to

$$\begin{aligned} n_1(l,t) &= \chi_m t^{-2}(l + \Gamma G\mu t)^{-2}, \\ \alpha t_{t_{\rm eq}} - \Gamma G\mu(t - t_{t_{\rm eq}}) < l &< \alpha t, \qquad t > t_{t_{\rm eq}}, \end{aligned} \tag{54}$$

with $\chi_m \approx 0.12\zeta$, with $\zeta \approx 4$ (see Table 10.1 in [3]). The lower bound on the length is due to the fact that the smallest loops present in the matter era started with a length $\alpha t_{\rm eq}$ when they were formed and their lengths have since decreased due to gravitational-wave emission. Additionally there are loops formed in the radiation era that survive into the matter era. Their lengths are distributed according to

$$\begin{aligned} n_2(l,t) &= \chi_r t_{\rm eq}^{1/2} t^{-2}(l + \Gamma G\mu t)^{-(5/2)}, \\ l < \alpha t_{t_{\rm eq}} - \Gamma G\mu(t - t_{t_{\rm eq}}), &\qquad t > t_{t_{\rm eq}}, \end{aligned} \tag{55}$$

where the upper bound on the length comes from the fact that the largest loops formed in the radiation era had a size $\alpha t_{\rm eq}$ but have since shrunk due to gravitational-wave emission.

The cusp spectrum has been calculated in [25] and the result shows that the spectrum is flat for *larger*[2] values of f. Later we will show that this is also the case for kink spectrum. This is rather unexpected since $\Omega(f)$ has an explicit $f^{-4/3}$ and $f^{-1/3}$ dependence for cusps and kinks, respectively. The only other f dependence comes from the Θ functions. In the following section we show analytically that the f dependence coming from the Θ function is of the form $f^{4/3}$ and $f^{1/3}$ for cusps and kinks, respectively, so that the spectrum is indeed flat for large values of the frequency f.

Before we start calculating the SBGW, we should mention a crucial observation due Damour and Vilenkin [20]. SBGW generated by a network of cosmic strings includes bursts which occur infrequently, and the computation of $\Omega_{\rm gw}(f)$ should not be biased by including these large rare events (i.e. events with low rate). If the loop density is taken of the form given in Eq. (48), the rate is specified by the redshift only. Therefore the condition on the rate can be implemented by a cutoff on redshifts such that large events for which the rate is smaller than the relevant time scale of the experiment are excluded (see Eq. (6.17) of [20]). However, when loops are large the situation is more complicated because at any given redshift there are loops of many different sizes given in Eqs. (53) and (54). This case has been dealt with in [25] as follows: instead of integrating over the variables l and z in Eq. (38) one integrates over h and z where h is defined in Eqs. (34) and (36) and imposes the cutoff limit on the h integral. The cutoff is defined as

$$\int_{h^*}^{\infty} dh \int dz \frac{d^2R}{dzdh} = f, \tag{56}$$

where $\frac{d^2R}{dzdh} = \frac{d^2R}{dzdl}\frac{dl}{dh}$. Equation (56) is solved for h^* and used to exclude rare events using the following integral [instead of Eq. (38)]:

$$\Omega_{\rm gw}(f) = \frac{4\pi^2}{3H_0^2} f^3 \int_0^{h^*} dh h^2 \int dz \frac{d^2R}{dzdh}. \tag{57}$$

This procedure removes large amplitude events (those with strain $h > h^*$) that occur at a rate smaller than f. Figure 1 shows the spectrum for kinks and cusps for small loops. For the top curves (red and green) we have $G\mu = 2 \times 10^{-6}$, $p = 10^{-3}$, and $\epsilon = 10^{-4}$, whereas for the bottom two curves (blue and pink) $G\mu = 10^{-7}$, $p = 5 \times 10^{-3}$ and $\epsilon = 1$ ($\epsilon \equiv \frac{\alpha}{\Gamma G\mu}$). Figure 2 shows the spectrum for large loops. For the top curves (blue and pink), which are almost identical, we have $G\mu = 10^{-7}$ and $p = 5 \times 10^{-3}$, whereas for the bottom two curves (red and green) $G\mu = 10^{-9}$ and $p = 5 \times 10^{-2}$. Here we note that for $f \gg \frac{H_0}{G\mu}$, the spectrum is flat for both cusps and kinks.

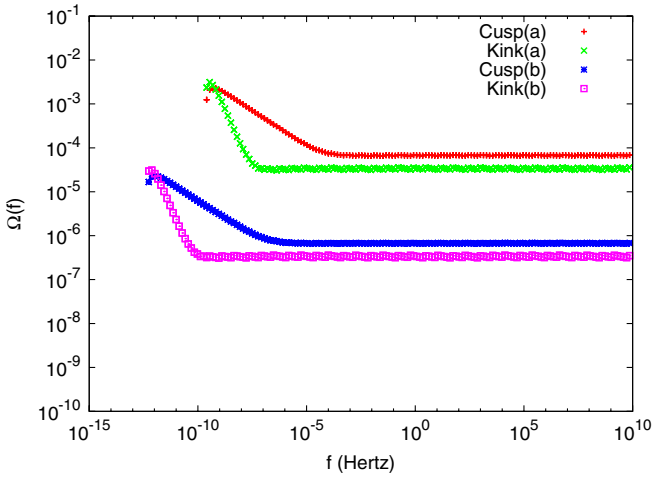

FIG. 1 (color online). Kink and cusp spectrum for small loops: (a) $G\mu = 2 \times 10^{-6}$, $p = 10^{-3}$ and $\epsilon = 10^{-4}$, (b) $G\mu = 10^{-7}$, $p = 5 \times 10^{-3}$ and $\epsilon = 1$.

[2] In the following section we show that the spectrum is flat for $f \gg \frac{H_0\sqrt{z_{\rm eq}}}{\alpha}$ for small loops and for $f \gg \frac{H_0\sqrt{z_{\rm eq}}}{G\mu\Gamma}$ for large loops.

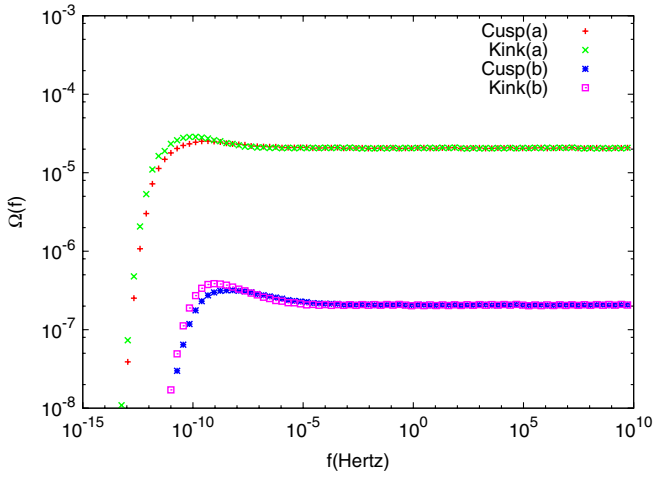

FIG. 2 (color online). Kink and cusp spectrum for large loops: (a) $G\mu = 10^{-7}$ and $p = 5 \times 10^{-3}$, (b) $G\mu = 10^{-9}$ and $p = 5 \times 10^{-2}$.

IV. ANALYTICAL APPROXIMATION FOR THE STOCHASTIC BACKGROUND

In this section we evaluate the spectrum analytically and show that the spectrum is constant for large values of f. Our main goal is to discuss the dependence of the spectrum on the parameters $G\mu$, $\epsilon \equiv \frac{\alpha}{\Gamma G\mu}$, and p for small loops and $G\mu$ and p for large loops. We limit our discussion to large values of f, for which the spectrum gets the dominant contribution from the loops in the radiation era. Matter era loops contribute to the lower frequency part of the spectrum.[3] Since we want to get an estimate of the spectrum we will neglect the complications arising from removing rare burst. In the radiation domination era, $z > z_{\rm eq} = \sqrt{\Omega_R} \simeq 5440$, the Hubble function in Eq. (33), can be approximated as

$$\mathcal{H}(z) \simeq \sqrt{\Omega_R} z^2 = \frac{z^2}{2\sqrt{z_{\rm eq}}}. \tag{58}$$

The cosmological functions that appear in the stochastic background radiation formula can be approximated as

$$\varphi_t(z) = \int_z^\infty \frac{dz'}{(1+z')\mathcal{H}(z')} \simeq \int_z^\infty \frac{dz'}{z'\mathcal{H}(z')} \simeq \sqrt{z_{\rm eq}} z^{-2}, \tag{59}$$

$$\varphi_r(z) = \int_0^z \frac{dz'}{\mathcal{H}(z')} = \int_0^{z_{\rm eq}} \frac{dz'}{\mathcal{H}(z')} + \int_{z_{\rm eq}}^z \frac{dz'}{\mathcal{H}(z')} \simeq 3.6, \tag{60}$$

$$\varphi_V(z) = \frac{4\pi\varphi_r^2}{(1+z)^3\mathcal{H}(z)} \simeq 325\sqrt{z_{\rm eq}} z^{-5}. \tag{61}$$

We first consider the small loop case, for which the expression for SBGW reduces to an integral over redshift given in Eqs. (51) and (52). Inserting the result in Eqs. (59)–(61) into Eq. (51) we get

$$\Omega_{gw,R}(f) \propto \frac{G\mu}{p\alpha^{1/3} f^{1/3}} \int_{z_{\rm eq}}^{z_{\rm max}} \frac{dz}{z^{2/3}} \Theta\left(1 - \left[\frac{f z_{\rm eq}^{1/2}\alpha}{H_0 z}\right]^{-(1/3)}\right) \propto \frac{G\mu}{p}, \tag{62}$$

where we dropped a term with $1/f$ dependence since it is small in the large f limit, and the subscript R reminds us that this is the contribution from radiation era loops. The upper limit of the integration, $z_{\rm max}$, is the redshift at the time of the creation of the strings, which depends on the energy scale of the phase transition. The result in Eq. (62) is valid for $\frac{z_{\rm eq}^{1/2}}{\alpha} \ll \frac{f}{H_0} < \frac{z_{\rm max}}{\alpha z_{\rm eq}^{1/2}}$, for which the upper limit of the integral is set by the Θ function. If $\frac{f}{H_0} > \frac{z_{\rm max}}{\alpha z_{\rm eq}^{1/2}}$, the integral does not depend on f and the frequency dependence of $\Omega_{gw,R}(f)$ is given by the prefactor, which has $f^{-1/3}$ behavior. For kinks we get

$$\Omega_{gw,R}^K(f) \propto \frac{G\mu}{p\alpha^{2/3} f^{2/3}} \int_{z_{\rm eq}}^{z_{\rm max}} \frac{dz}{z^{1/3}} \Theta\left(1 - \left[\frac{f z_{\rm eq}^{1/2}\alpha}{H_0 z}\right]^{-(1/3)}\right) \propto \frac{G\mu}{p}. \tag{63}$$

Equations (62) and (63) show that for $\frac{z_{\rm eq}^{1/2}}{\alpha} \ll \frac{f}{H_0}$ the spectrum is constant and it scales with $G\mu/p$. The amplitude does not depend on the parameter α, however the spectrum shifts to the right linearly in α.

This result is in perfect agreement with Fig. 1. For the bottom curves $\frac{G\mu}{p} = 2 \times 10^{-5}$ where as $\frac{G\mu}{p} = 2 \times 10^{-3}$ for the top curves, which have 2 orders of magnitude larger amplitude, exactly agreeing with the figure. Furthermore, the top curves ($\epsilon = 10^{-4}$) are shifted to the right compared to the bottom curves ($\epsilon = 1$) by about 4 orders in f as predicted by our results above.

Now we consider large loops in the radiation domination era, for which the density $n(l, t)$ is given in Eq. (53), where t is to be replaced with $\varphi_t(z)/H_0$. Substituting the results in Eqs. (59)–(61) into Eq. (38) we get

[3] It is relatively easier to verify this in the case of small loops. If one limits the redshift integration in Eqs. (62) and (63) to matter domination and uses the corresponding approximate cosmological functions, it is found that $\Omega(f)$ depends on the negative powers of f, which are negligible for large f. The same argument also applies to the large loop case.

$$\Omega_{gw,R}(f) = A(f)\int dz \int dl \frac{z(lz)^{-(1/3)}}{(lz^2+\beta\delta)^{(5/2)}}\Theta\left(1-\frac{1}{fzl}\right) \times \Theta\left(\frac{\beta}{z^2}-l\right) = A(f)\int_{z_{\rm eq}}^{z^*} dz \int_{1/f}^{\beta/z} du \frac{u^{-(1/3)}}{(uz+\beta\delta)^{5/2}}, \quad (64)$$

where we define

$$A(f) = \frac{165 c\alpha^2\delta^2\chi_R}{p z_{\rm eq}^{1/4} H_0^{3/2}\Gamma^2 f^{1/3}}, \quad (65)$$

with $\delta = \frac{G\mu\Gamma}{\alpha}$ and $\beta = \frac{\alpha\sqrt{z_{\rm eq}}}{H_0}$ ($\alpha \approx 0.1$ for large loop case) and the dummy integration variable $u = lz$. The upper limit of the z integral, z^*, will be set by requiring $\beta/z > 1/f$, that is, $z < f\beta$. If $f < z_{\rm max}/\beta$, we have

$$\Omega(f) = A(f)\int_{z_{\rm eq}}^{\beta/f} dz \int_{1/f}^{\beta/z} du \frac{u^{-1/3}}{(uz+\beta\delta)^{5/2}} = A(f)\int_{1/f}^{\beta/z_{\rm eq}} du \int_{z_{\rm eq}}^{\beta/u} dz \frac{u^{-(1/3)}}{(uz+\beta\delta)^{5/2}} = -\frac{2}{3}A(f)\int_{1/f}^{\beta/z_{\rm eq}} \frac{du}{u^{4/3}}\left(\frac{1}{(\beta+\beta\delta)^{3/2}} - \frac{1}{(uz_{\rm eq}+\beta\delta)^{3/2}}\right). \quad (66)$$

If $\frac{1}{f} < \frac{\delta\beta}{z_{\rm eq}} = \frac{G\mu\Gamma}{H_0\sqrt{z_{\rm eq}}}$, we can split the integration range $[1/f, \beta/z_{\rm eq}]$ in the second integral into $[1/f, \delta\beta/z_{\rm eq}]$ and $[\delta\beta/z_{\rm eq}, \beta/z_{\rm eq}]$ and neglect $uz_{\rm eq}$ and $\beta\delta$ respectively in these two integrals. Combining all terms and keeping the lowest order in δ we get

$$\Omega_{gw,R}(f) = A(f)\left(\frac{2f^{1/3}}{(\delta\beta)^{3/2}} - \frac{18 z_{\rm eq}^{1/3}}{11(\delta\beta)^{11/6}}\right) = \frac{330 c\alpha^2\delta^{1/2}\chi_R}{p z_{\rm eq}^{1/4} H_0^{3/2}\Gamma^2\beta^{3/2}} \simeq 3.2\times 10^{-4}\frac{\sqrt{G\mu}}{p}, \quad f > \frac{3.6\times 10^{-18}}{G\mu}\ \text{Hz}. \quad (67)$$

The calculation for the case of kink is very similar to cusp case, following the same steps we get

$$\Omega^K_{gw,R}(f) \simeq 3.2\times 10^{-4}\frac{\sqrt{G\mu}}{p}, \qquad f > \frac{3.6\times 10^{-18}}{G\mu}\ \text{Hz}, \quad (68)$$

which is identical to the cusp result. Equations (67) and (68) show that the distribution is flat for $f > \frac{3.6\times 10^{-18}}{G\mu}$ Hz and its amplitude scales with $\sqrt{G\mu}/p$, which is in excellent agreement with Fig. 2. The flat value of the spectrum for the top curves ($G\mu = 10^{-7}$ and $p = 5\times 10^{-3}$) is 2.1×10^{-5} and for the bottom curve ($G\mu = 10^{-9}$ and $p = 5\times 10^{-2}$) is 2.1×10^{-7}. These results are to be compared with the analytical results 2.0×10^{-5} and 2.0×10^{-7} predicted by Eqs. (67) and (68).

It is important to note that, in this paper we assume that the number of kinks, N, is order of 1. This assumption enters in the estimation $|\ddot{X}_\pm| \sim \frac{2\pi}{l}$, and if there are N kinks on strings, it needs to be replaced by $|\ddot{X}_\pm| \sim \frac{2\pi}{l/N}$. The replacement of l with l/N should also be done in the opening angle of the cone of the radiation, Eq. (37), which will result in a nontrivial dependence on N. However we can simply convert the resultant expression to the one we calculated in Eq. (52) by defining $\alpha = \alpha' N$. Since we have shown that α has the effect of moving the spectrum horizontally, one effect of having N kinks will be shifted spectrum compared to one kink spectrum. The other effect will be an overall scaling of the spectrum by $1/N$.

V. PARAMETER SPACE CONSTRAINTS AND RESULTS

In this section we discuss certain experimental bounds on SBGW. For the case of large loops the parameters are $G\mu$ and p, and for small loops the parameters are $G\mu$, ϵ, and p. It is important to note that the nontrivial dependence on p follows from excluding rare bursts as described in Eqs. (56) and (57) [if rare events were included $\Omega(f)$ would simply scale with $1/p$].

Accessible regions corresponding to different experiments and bounds are shown in Fig. 3. The shaded regions, from darkest to lightest, are: LIGO S4 [33] limit, LIGO S5 [34], LIGO H1H2 projected sensitivity (cross-correlating the data from the two LIGO interferometers at Hanford, Washington, [H1 and H2]), and AdvLIGO H1H2 projected sensitivity. All projections assume 1 yr of exposure and either LIGO design sensitivity or advanced LIGO sensitivity tuned for binary neutron star inspiral search. The solid black curve corresponds to the big-bang nucleosynthesis (BBN) [35] bound, the dot-dashed curve to the pulsar bound [36], the +s to the projected pulsar sensitivity, the circles to the bound based on the cosmic microwave background (CMB) and matter spectra [37], the ×s to the projected sensitivity of the LIGO burst [22] search, and the ◇-curve to the LISA projected sensitivity [38]. The BBN and CMB bounds are integral bounds, i.e. they are upper limits for the integral of $\Omega(f)$ over $\ln f$, therefore a model is excluded if it predicts an integral larger than the limit. On the other hand, the pulsar and LIGO bounds apply in specific frequency bands, thus a model is excluded if it has $\Omega(f)$ larger than the limit (or projected sensitivity) for any f in the range of the pulsar or LIGO experiments. The range of the redshift integral in Eq. (38) must be chosen properly for a given experiment. For the BBN bound, the integration is performed for $z > 5.5\times 10^9$. Similarly, for the bound based on the CMB and matter spectra, the integration is performed for $z > 1100$. First, we note that smaller values of p are more accessible, which follows

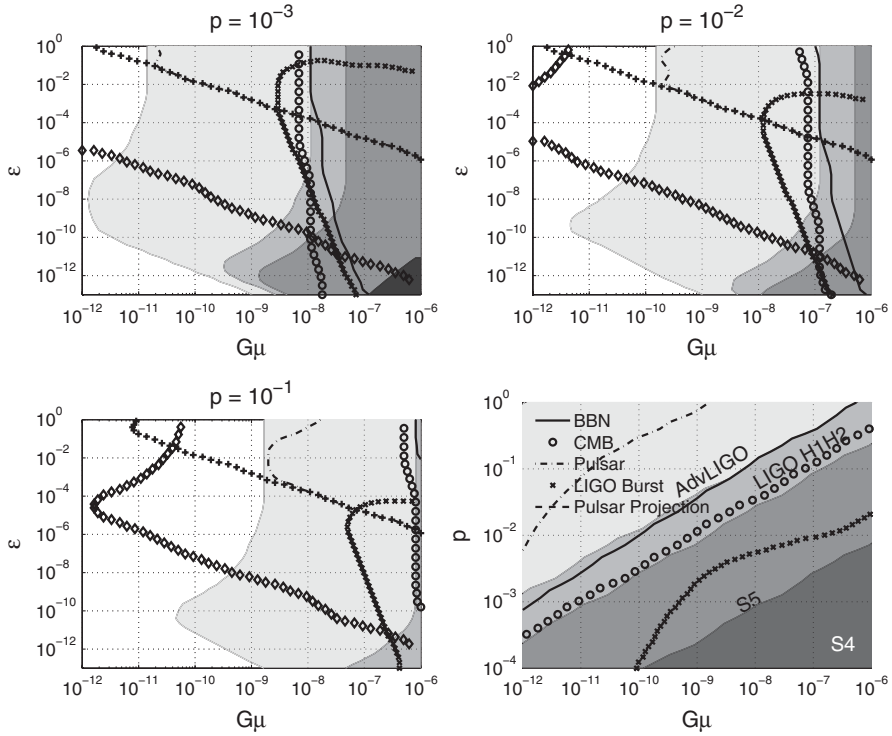

FIG. 3. Top-left: Accessible regions in the $\varepsilon - G\mu$ plane for $p = 10^{-3}$ for small loops (loop sizes are determined by gravitational backreaction). Top-right: Same as above for $p = 10^{-2}$. Bottom-left: Same as above for $p = 10^{-1}$. Bottom-right: Accessible regions in the $p - G\mu$ plane for the large long-lived loop models. The accessible regions are to the right of the corresponding curves. All models are within reach of LISA and advanced LIGO, and most are within the projected pulsar bound.

from the fact that the loop density is inversely proportional to p. This makes cosmic superstrings more accessible than field theoretical strings. Second, we note that the LIGO stochastic search constrains the large $G\mu$, small ϵ part of the parameter space, whereas the pulsar limit constrainsthe large $G\mu$ and large ϵ part of the parameter space. Similarly, the LIGO burst bound applies to the large $G\mu$ and intermediate ϵ part of the parameter space. Therefore the large $G\mu$ part of the parameter space is covered by these three experiments. Furthermore since they also overlap for large $G\mu$ and intermediate ϵ, in the case of detection, the two LIGO searches could potentially confirm each other. We also see that the BBN and CMB bounds are not very sensitive to ϵ: the corresponding curves are rather vertical in $\epsilon - G\mu$ plane. This result is in perfect agreement with our results [Eqs. (62) and (63)] that show $\Omega(f) \propto G\mu/p$, which does not depend on ϵ. For the case of large loops, the gravitational-wave background is significantly larger than the small loop one; see Figs. 1 and 2. Therefore more of the parameter space is accessible to the current and proposed experiments, as depicted in the right bottom panel of Fig. 3. The strongest constraint is the pulsar bound, which rules out cosmic (super)string models with $G\mu > 10^{-12}$ and $p < 8 \times 10^{-3}$. This bound also rules out field theoretical strings ($p = 1$) with $G\mu > 2 \times 10^{-9}$. One can compare these results with the case where only cusps are included [25]. In that case cosmic (super) string models with $G\mu > 10^{-12}$ and $p < 3 \times 10^{-3}$ and field theoretical strings with $G\mu > 10^{-9}$ are ruled out. This result illustrates that kinks contribute to SBGW at the same order as cusps.

ACKNOWLEDGMENTS

We would like to thank Marco Peloso for useful discussions. S. Ö. is supported by the Graduate School at the University of Minnesota, X. S. is supported in part by NSF Grant No. PHY-0758155 and the Research Growth Initiative at the University of Wisconsin-Milwaukee, and V. M. is supported in part by NSF Grant No. PHY0758036.

[1] H. B. Nielsen and P. Olesen, Nucl. Phys. **B61**, 45 (1973).

[2] T. W. B. Kibble, J. Phys. A **9**, 1387 (1976).

[3] A. Vilenkin and E. Shellard, *Cosmic Strings and Other Topological Defects* (Cambridge University Press, Cambridge, England, 2000).
[4] R. Jeannerot, J. Rocher, and M. Sakellariadou, Phys. Rev. D **68**, 103514 (2003).
[5] Y. B. Zeldovich, Mon. Not. R. Astron. Soc. **192**, 663 (1980).
[6] A. Vilenkin, Phys. Rev. Lett. **46**, 1169 (1981); **46**, 1496(E) (1981).
[7] M. R. Anderson, *The Mathematical Theory of Cosmic Strings* (Institute of Physics Publishing, London, 2003).
[8] V. A. Gasilov, V. I. Maslyankin, and M. Yu. Khlopov, Astrofiz. **23**, 191 (1985) [Astrophysics **23**, 485 (1986)].
[9] M. V. Sazhin and M. Yu. Khlopov, Astron. Zh. **66**, 191 (1989) [Sov. Astron. **33**, 98 (1989)].
[10] N. Jones *et al.*, J. High Energy Phys. 07 (2002) 051; S. Sarangi and S. H. Henry Tye, Phys. Lett. B **536**, 185 (2002); G. Dvali and A. Vilenkin, J. Cosmol. Astropart. Phys. 03 (2004) 010; N. Jones *et al.*, Phys. Lett. B **563**, 6 (2003); E. J. Copeland *et al.*, J. High Energy Phys. 06 (2004) 013.
[11] M. Eto, K. Hashimoto, G. Marmorini, M. Nitta, K. Ohashi, and W. Vinci, J. Cosmol. Astropart. Phys. 09 (2005) 004.
[12] G. Dvali and A. Vilenkin, J. Cosmol. Astropart. Phys. 03 (2004) 010.
[13] M. G. Jackson, N. T. Jones, and J. Polchinski, J. High Energy Phys. 10 (2005) 013.
[14] L. Leblond, B. Shlaer, and X. Siemens, Phys. Rev. D **79**, 123519 (2009).
[15] N. Jones, H. Stoica, and S. H. Henry Tye, Phys. Lett. B **563**, 6 (2003).
[16] M. Sakellariadou, J. Cosmol. Astropart. Phys. 04 (2005) 003.
[17] A. Avgoustidis and E. P. S. Shellard, Phys. Rev. D **73**, 041301 (2006).
[18] L. Pogosian, M. C. Wyman, and I. Wasserman, J. Cosmol. Astropart. Phys. 09 (2004) 008.
[19] E. Jeong and G. F. Smoot, Astrophys. J. **624**, 21 (2005).
[20] T. Damour and A. Vilenkin, Phys. Rev. Lett. **85**, 3761 (2000).
[21] T. Damour and A. Vilenkin, Phys. Rev. D **64**, 064008 (2001).
[22] X. Siemens *et al.*, Phys. Rev. D **73**, 105001 (2006).
[23] J. Polchinski, AIP Conf. Proc. **743**, 331 (2004); J. Polchinski, arXiv:hep-th/0412244.
[24] B. P. Abbott *et al.* (LIGO Scientific Collaboration), Phys. Rev. D **80**, 062002 (2009).
[25] X. Siemens, V. Mandic, and J. Creighton, Phys. Rev. Lett. **98**, 111101 (2007).
[26] M. Kawasaki, K. Miyamoto, and K. Nakayama, arXiv: astro-ph/1002.0652.
[27] M. Kawasaki, K. Miyamoto, and K. Nakayama, arXiv: astro-ph/1003.3701.
[28] S. Weinberg, *Gravitation and Cosmology* (Wiley, New York, 1972).
[29] E. J. Copeland and T. W. B. Kibble, Phys. Rev. D **80**, 123523 (2009).
[30] C. Ringeval, M. Sakellaridou, and F. Bouchet, arXiv:astro-ph/0511646.
[31] C. J. A. P. Martins and E. P. S. Shellard, Phys. Rev. D **73**, 043515 (2006).
[32] V. Vanchurin, K. D. Olum, and A. Vilenkin, Phys. Rev. D **74**, 063527 (2006).
[33] B. Abbott *et al.*, Astrophys. J. **659**, 918 (2007).
[34] B. P. Abbott *et al.* (LIGO and Virgo Collaborations), Nature (London) **460**, 990 (2009).
[35] R. H. Cyburt *et al.*, Astropart. Phys. **23**, 313 (2005).
[36] F. A. Jenet *et al.*, Astrophys. J. **653**, 1571 (2006).
[37] T. L. Smith, E. Pierpaoli, and M. Kamionkowski, Phys. Rev. Lett. **97**, 021301 (2006).
[38] P. L. Bender and K. Danzmann (The LISA Study Team), the LISA Project Report No. MPQ233, 1998 (unpublished).